Letter Vol. 44, No. 8 / 15 April 2019 / Optics Letters 2097

Optics Letters

Noise suppression technique for distributed Brillouin sensing with polymer optical fibers

Yosuke Mizuno,[1,*] Heeyoung Lee,[1] Neisei Hayashi,[2] and Kentaro Nakamura[1]

[1]Institute of Innovative Research, Tokyo Institute of Technology, Yokohama 226-8503, Japan
[2]Research Center for Advanced Science and Technology, The University of Tokyo, Tokyo 153-8904, Japan
*Corresponding author: ymizuno@sonic.pi.titech.ac.jp

Received 15 January 2019; revised 18 March 2019; accepted 19 March 2019; posted 22 March 2019 (Doc. ID 357498); published 15 April 2019

We develop a new noise suppression technique to perform distributed strain and temperature sensing based on a higher-speed configuration of Brillouin optical correlation-domain reflectometry even when a polymer optical fiber (POF) is used as a sensing fiber. We acquire the spectral difference between with and without reference light, leading to selective observation of the beat signal of Brillouin-scattered light and reference light, which is effective for distributed sensing. After experimentally showing the usefulness of this technique, we demonstrate POF-based distributed temperature sensing and dynamic strain sensing.

https://doi.org/10.1364/OL.44.002097

Brillouin scattering in optical fibers has been exploited to develop distributed strain and temperature sensors [1]. Such sensors are categorized into two configurations: one is two-end-access "analysis," which includes Brillouin optical time- [2,3], frequency- [4], and correlation-domain [5,6] analysis (BOTDA, BOFDA, and BOCDA); the other is single-end-access "reflectometry," which includes Brillouin optical time- [7], frequency- [8], and correlation-domain [9] reflectometry (BOTDR, BOFDR, and BOCDR). Combination of some of these configurations has also been developed [10,11]. Different configurations have different advantages and disadvantages, and here we focus on BOCDR [9], which has advantages such as operation by single-end light injection, relatively high spatial resolution, random accessibility, and high cost efficiency. One of the major disadvantages of a standard BOCDR configuration is its long measurement time caused by frequency sweeping required to obtain a Brillouin gain spectrum (BGS) at each measurement position. The sampling rate of the standard configuration was limited to 19 Hz when a silica single-mode fiber (SMF) was used as a fiber under test (FUT) [12]. To enhance the flexibility of the FUT, some researchers [13–16] have made attempts to use polymer optical fibers (POFs) for Brillouin sensing. To date, a 0.1 m heated section of a 1.3 m POF has been detected using a standard BOCDR configuration, but the sampling rate was limited to 3.3 Hz because of the low signal-to-noise ratio (SNR) [16].

To boost the sampling rate of BOCDR and demonstrate real-time distributed sensing, we recently developed a frequency-sweeping-free configuration named phase-detected BOCDR and achieved a sampling rate of >100 kHz [17]. However, the maximal measurable strain was limited to 0.2%. Another frequency-sweeping-free configuration named slope-assisted BOCDR has also been developed, but its strain dynamic range was also limited to <0.3% [18]. To extend the strain dynamic range to >2.0% (close to fracture strain of silica fibers), still another BOCDR configuration with higher-speed frequency sweeping has been developed, and its usefulness has been proved using a silica SMF as an FUT [19].

In this higher-speed configuration, the noise floor was suppressed by acquiring the spectral difference between with and without pump light. When the FUT was a silica SMF, the electrical noise was then mitigated, and distributed measurement was correctly performed [19]. However, when the FUT was a POF, the Fresnel reflection at the SMF-to-POF boundary was so strong that, even though the electrical noise was mitigated as expected, the final signal involved not only the beat signal of Brillouin-scattered light and reference light (effective for distributed measurement) but also the beat signal of Brillouin-scattered light and the Fresnel-reflected light (not effective). As the latter beat signal is sometimes extremely strong [20], it was difficult to directly employ this higher-speed configuration to perform POF-based distributed sensing.

In this study, we develop a new noise suppression technique to appropriately perform distributed sensing based on higher-speed BOCDR even when the FUT is a POF. By acquiring the spectral difference between with and without reference light (not pump light), we selectively observe the beat signal of Brillouin-scattered light and reference light, removing the influence of the beat signal of Brillouin-scattered light and Fresnel-reflected light. We experimentally show the effectiveness of this technique and demonstrate POF-based distributed temperature sensing and dynamic strain sensing.

BOCDR is a fiber-optic distributed Brillouin sensing technique based on synthesis of optical coherence functions [9,21,22]. By sinusoidally modulating the driving current of the laser, its output frequency is also modulated, generating a so-called correlation peak (corresponding to a measurement position) in an FUT. By sweeping the modulation frequency, the location of the correlation peak can be scanned along the FUT, enabling distributed measurement. The spatial resolution, Δz, and the measurement range, d_m, are given by [9,21]

$$\Delta z = \frac{c \Delta \nu_B}{2\pi n f_m \Delta f}, \tag{1}$$

$$d_m = \frac{c}{2 n f_m}, \tag{2}$$

where c is the velocity of light in a vacuum, $\Delta \nu_B$ is the Brillouin bandwidth, n is the refractive index of the fiber core, f_m is the modulation frequency, and Δf is the modulation amplitude of the optical frequency. The upper limit of Δf is known to be half the Brillouin frequency shift (BFS) [9,21]. In a standard BOCDR configuration, the sampling rate was limited to 19 Hz by the frequency-sweeping speed of an electrical spectrum analyser (ESA). To enhance the sampling rate while maintaining the strain dynamic range, we have developed a new configuration of BOCDR with higher-speed frequency sweeping [19].

In the higher-speed BOCDR, the BGS is converted from the frequency domain to the time domain for higher-speed processing. First, the Brillouin-scattered signal is heterodyned with the reference light and experiences optical-to-electrical conversion using a photo detector (PD). The Brillouin signal is then mixed with the output of a microwave frequency sweeper (MFS), the frequency of which is repeatedly swept for several hundred megahertz to scan the BGS in the frequency domain. Subsequently, the power at a fixed frequency component of the mixed signal is output from the ESA using a zero-span mode, and the BGS is repeatedly reproduced in the time domain. The BGS acquisition must be slower than the calculation time required for the BFS derivation from the BGS, which limits the maximal sampling rate of this configuration. Finally, the BGS signal in the time domain is input to a computer via a sound board and monitored using a virtual oscilloscope triggered at the repetition frequency of the MFS.

Conventionally, to suppress the noise floor, we acquired the spectral difference between with and without the pump light. When the pump light is injected into the FUT, the heterodyned signal at the PD is composed of three factors: (i) the beat signal of the Brillouin-scattered light and reference light, (ii) the beat signal of the Brillouin-scattered light and Fresnel-reflected light, and (iii) the electrical noise. The spectral shape of (i) varies according to the location of the correlation peak and is effective for distributed measurement. In contrast, (ii) does not vary according to the location of the correlation peak and serves as noise in distributed measurement. (iii) is the electrical noise mainly caused by the output-power fluctuations of the MFS accompanied by frequency sweeping. In the meantime, when the pump light is not injected in the FUT, only (iii) is included in the observed spectrum. Therefore, by calculating the spectral difference, the final spectrum includes (i) and (ii). When the FUT is a silica SMF, the Fresnel-reflected light is extremely weak (note that, in previous experiments, the distal end of the FUT was cut with an angle [19]) and thus (ii) is negligibly small. Therefore, by using the spectral difference between with and without the pump light, silica-SMF-based distributed measurements have been successfully demonstrated in the higher-speed BOCDR configuration [19].

However, when the FUT is a POF, the Fresnel reflection at the boundary of a silica SMF (second port of an optical circulator) and the POF is so strong that (ii) is not negligible (this can be interpreted as a pseudo-correlation peak [23], which is universally located at the proximal POF end). Considering that the pump power is generally high (e.g., >20 dBm), (ii) is sometimes larger than (i). Therefore, the final spectrum includes both (i), which is effective, and (ii), which is not effective, leading to difficulty in performing POF-based distributed sensing with this conventional technique. Note that insertion of a tapered fiber between the SMF and the POF cannot completely suppress the Fresnel reflection.

To tackle this problem, we develop a new noise suppression technique for POF-based distributed sensing. Here we acquire the spectral difference with and without the reference light, not the pump light. When the reference light is present, the final spectrum includes (i), (ii), and (iii); while the reference light is not present, it includes (ii) and (iii). Therefore, their difference gives only (i), which directly contributes to distributed sensing. Note that this technique is applicable not only to POFs but also standard silica SMFs.

Figure 1 schematically shows the experimental setup of POF-based BOCDR for verifying the new noise suppression technique. The basic structure of the setup is the same as previously reported [9,21]. A 3.0 m perfluorinated graded-index POF [24] with a core diameter of 50 μm was employed as the FUT. It had a propagation loss of ∼0.25 dB/m at 1550 nm, a BFS of 2.85 GHz at 1550 nm [25], and its strain and temperature dependence coefficients were −121.8 MHz/% [26] and −3.2 MHz/°C [27], respectively. The SMF of the second port of the optical circulator was 0.8 m in length and was connected to the POF by butt-coupling [25]. The other end of the POF was cut with an 8° angle. The pump light was amplified using an erbium-doped fiber amplifier (EDFA), and its power injected into the FUT was 22 dBm. The power of the reference light was 4 dBm (before being injected into the final optical coupler). Variable optical attenuators (VOAs) were newly inserted in the pump and the reference path following EDFAs so that they were used to switch on/off the pump light and the reference light for the noise suppression.

First, we evaluated the conventional noise suppression technique by acquiring the spectral difference between with and without the pump light. The correlation peak was located at the midpoint of the FUT ($f_m = 13.552$ MHz), and the nominal spatial resolution was set to approximately 0.65 m ($\Delta f = 0.4$ GHz). The spectra measured with and without the pump light are shown in Figs. 2 and 3(a), respectively. Figure 2 exhibited a clear BGS peak, but the spectrum was distorted by the electrical noise. Figure 3(a) shows the electrical

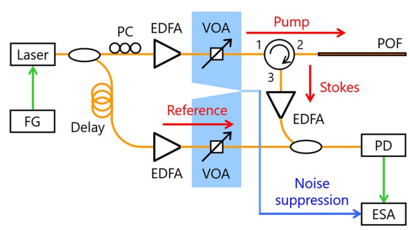

Fig. 1. Experimental setup including a polymer optical fiber (POF) for verifying the new noise suppression technique. EDFA, erbium-doped fiber amplifier; ESA, electrical spectrum analyzer; FG, function generator; PC, polarization controller; PD, photo detector; VOA, variable optical attenuator.

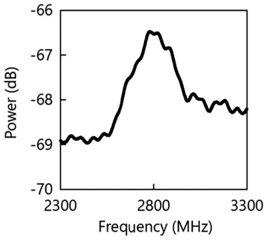

Fig. 2. Measured raw BGS.

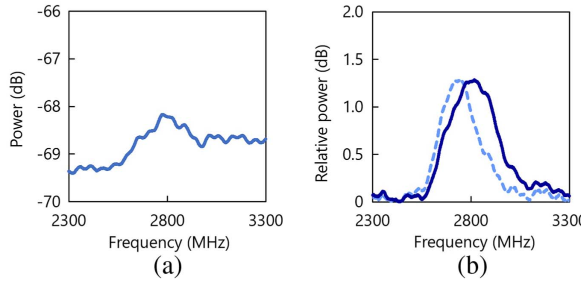

Fig. 4. Spectra measured with the new noise suppression technique. (a) Noise floor. (b) Noise-suppressed BGS. The dotted curve is the spectrum when a 0.6% strain was applied.

noise spectrum, which did not include a clear BGS peak. The spectral difference of these two, obtained using a calculating function of the ESA, is shown as a solid curve in Fig. 3(b) [note that the three spectra were not simultaneously obtained and that the direct subtraction of Fig. 3(a) from Fig. 2 slightly differs from Fig. 3(b)]. As the electrical noise was suppressed, the spectral shape seemed to be ideal, but this spectrum cannot be directly used for distributed measurement. To clarify this issue, a 0.6% strain was applied to a 1.0 m section around the midpoint of the FUT where the correlation peak was located. The spectrum then shifted to lower frequency, as indicated by a dotted curve in Fig. 3(b). However, the downshift of the peak frequency was ~33 MHz (calculated after Lorentzian fitting), which was lower than half the theoretical value (~73 MHz; calculated using the aforementioned strain dependence coefficient of the BFS in the POF). This is because, as strain was applied, part of the spectrum [corresponding to (i)] shifted to lower frequency, but the remaining part of the spectrum [corresponding to (ii)] did not shift. Consequently, the overlap of these two spectra yielded a slightly shifted spectrum. Thus, it is difficult to use the conventional noise suppression technique to derive the correct value of the BFS change caused by strain.

Subsequently, under the same measurement conditions, we evaluated the new noise suppression technique by acquiring the spectral difference between with and without the reference light. The spectrum measured with the reference light is basically the same as Fig. 2. The spectrum measured without the reference light is shown in Fig. 4(a), which included not only the electrical noise spectrum but also a clear BGS peak. This peak corresponds to (ii) and does not contribute to distributed measurement. The spectral difference of these two is shown as a solid curve in Fig. 4(b). It is natural that the height of the spectrum is lower than that in Fig. 3(b), because the whole spectrum is effective for distributed sensing in Fig. 4(b). To prove this, a 0.6% strain was applied in the same manner, and the shifted spectrum is shown as a dotted curve in Fig. 4(b). Compared to Fig. 3(b), as strain was applied, the whole spectrum shifted to lower frequency, and the shift of the peak frequency was ~73 MHz (calculated after Lorentzian fitting), which was in good agreement with the theoretical value. Thus, the new noise suppression technique was proven to give a correct value of the BFS change caused by applied strain. This indicates that the new technique is inherently superior to the conventional one for distributed sensing. Note that, if the BGS of the whole length of the POF is to be analyzed, the conventional technique is more suitable considering its seemingly higher SNR.

Finally, we performed two demonstrations of POF-based higher-speed BOCDR using the new noise suppression technique. The setup was very similar to that which was previously reported [19]. The length of the POF was 3.0 m. The modulation frequency f_m was swept from 13.515 to 13.590 MHz (corresponding to the measurement range of ~8.2 m), and the modulation amplitude Δf was ~0.4 GHz (corresponding to the nominal spatial resolution of ~0.65 m). The sampling rate was 42 Hz, which cannot be achieved using a standard BOCDR configuration. The room temperature was 25°C. In the first demonstration, a 1.0-m-long section of the POF was heated to 55°C [Fig. 5(a)]. The measured BGS (normalized) and BFS distributions are shown in Figs. 5(b) and 5(c),

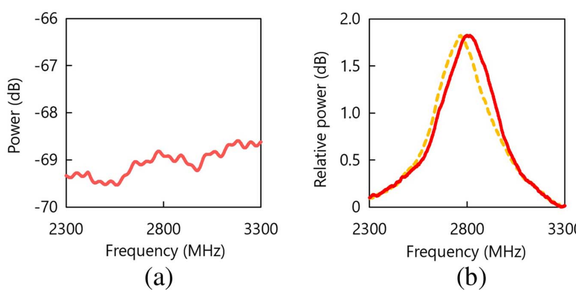

Fig. 3. Spectra measured with the conventional noise suppression technique. (a) Noise floor. (b) Noise-suppressed BGS. The dotted curve is the spectrum when a 0.6% strain was applied.

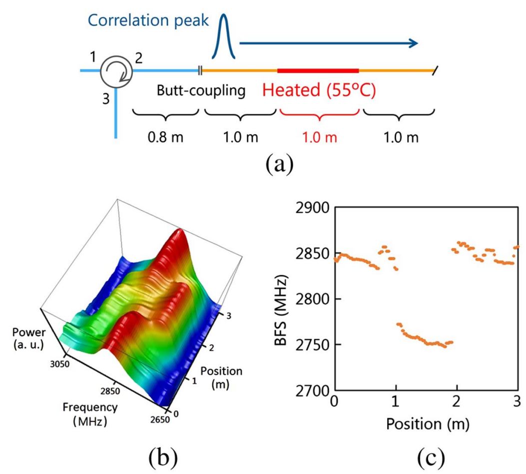

Fig. 5. Demonstration of distributed temperature sensing. (a) Structure of the FUT. Measured distributions of (b) BGS and (c) BFS.

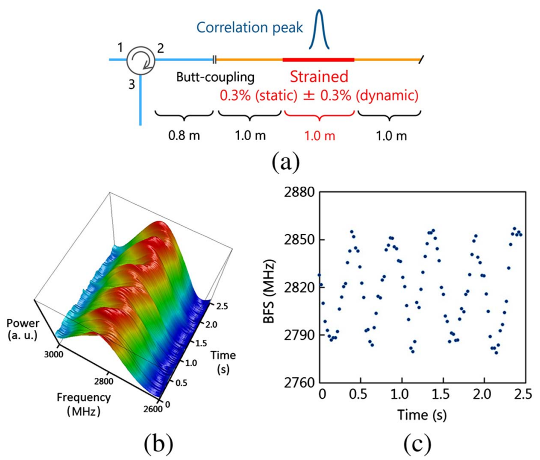

Fig. 6. Demonstration of dynamic strain sensing. (a) Structure of the FUT. Measured temporal variations of (b) BGS and (c) BFS.

respectively. The number of the measured points were 84 and no averaging was performed, resulting in the measurement time of 2 s. The error of the BFS measurement (calculated as a standard deviation of the BFS values along the non-strained sections) was approximately ±4 MHz in this demonstration. The frequency downshift at the heated section was roughly 100 MHz, which well agreed with the theoretical value (~96 MHz). Thus, distributed measurement was correctly performed. The BFS fluctuations can be mitigated by averaging at the cost of the measurement time. In the second demonstration, by setting the modulation frequency f_m to 13.552 MHz, the correlation peak was located at the midpoint of the POF. A 0.3% static strain was applied in advance to a 1.0-m-long section around it, and then a dynamic strain of ±0.3% was sinusoidally applied at 2.0 Hz to the pre-strained section [Fig. 6(a)]. The measured temporal variations of the BGS (normalized) and the BFS are shown in Figs. 6(b) and 6(c), respectively. The amplitude of the BFS variation was roughly 35 MHz, which agreed with the theoretical value (~37 MHz). Thus, a dynamic strain at 2.0 Hz was correctly measured with the new noise suppression technique. The sampling rate can be enhanced to several hundreds of hertz simply by replacing the MFS with a voltage-controlled oscillator (or another MFS with a higher frequency-sweeping rate).

In conclusion, we developed a new noise suppression technique for POF-based distributed strain/temperature sensing based on higher-speed BOCDR. This technique is not suitable for non-distributed measurement; namely, the conventional technique is more suitable for the BGS analysis of the whole length of the POF because of its higher SNR. However, the new technique has an effect of SNR enhancement even when the FUT is a silica SMF because non-zero optical reflection is caused also at an SMF-to-SMF boundary. Thus, we anticipate that the new technique will be one of the most fundamental tools for BOCDR-based distributed sensing, especially when a POF is employed as an FUT, in the near future.

Funding. Japan Society for the Promotion of Science (JSPS) (17H04930, 17J07226); Fujikura Foundation.

REFERENCES

1. A. Motil, A. Bergman, and M. Tur, Opt. Laser Technol. **78**, 81 (2016).
2. T. Horiguchi and M. Tateda, J. Lightwave Technol. **7**, 1170 (1989).
3. A. Denisov, M. A. Soto, and L. Thévenaz, Light: Sci. Appl. **5**, e16074 (2016).
4. D. Garus, K. Krebber, F. Schliep, and T. Gogolla, Opt. Lett. **21**, 1402 (1996).
5. K. Hotate and T. Hasegawa, IEICE Trans. Electron. **83**, 405 (2000).
6. Y. H. Kim, K. Lee, and K. Y. Song, Opt. Express **23**, 33241 (2015).
7. T. Kurashima, T. Horiguchi, H. Izumita, S. Furukawa, and Y. Koyamada, IEICE Trans. Commun. **76**, 382 (1993).
8. A. Minardo, R. Bernini, R. Ruiz-Lombera, J. Mirapeix, J. M. Lopez-Higuera, and L. Zeni, Opt. Express **24**, 29994 (2016).
9. Y. Mizuno, W. Zou, Z. He, and K. Hotate, Opt. Express **16**, 12148 (2008).
10. Y. Mizuno, Z. He, and K. Hotate, Opt. Express **17**, 9040 (2009).
11. D. Elooz, Y. Antman, N. Levanon, and A. Zadok, Opt. Express **22**, 6453 (2014).
12. Y. Mizuno, Z. He, and K. Hotate, IEEE Photon. Technol. Lett. **21**, 474 (2009).
13. A. Minardo, R. Bernini, and L. Zeni, IEEE Photon. Technol. Lett. **26**, 387 (2014).
14. A. Schreier, A. Wosniok, S. Liehr, and K. Krebber, Opt. Express **26**, 22307 (2018).
15. Y. Dong, P. Xu, H. Zhang, Z. Lu, L. Chen, and X. Bao, Opt. Express **22**, 26510 (2014).
16. N. Hayashi, Y. Mizuno, and K. Nakamura, J. Lightwave Technol. **32**, 3999 (2014).
17. Y. Mizuno, N. Hayashi, H. Fukuda, K. Y. Song, and K. Nakamura, Light: Sci. Appl. **5**, e16184 (2016).
18. H. Lee, N. Hayashi, Y. Mizuno, and K. Nakamura, IEEE Photon. J. **8**, 6802807 (2016).
19. Y. Mizuno, N. Hayashi, H. Fukuda, and K. Nakamura, Jpn. J. Appl. Phys. **56**, 072501 (2017).
20. Y. Mizuno, N. Hayashi, and K. Nakamura, Electron. Lett. **50**, 1153 (2014).
21. Y. Mizuno, W. Zou, Z. He, and K. Hotate, J. Lightwave Technol. **28**, 3300 (2010).
22. K. Hotate, Meas. Sci. Technol. **13**, 1746 (2002).
23. N. Hayashi, Y. Mizuno, and K. Nakamura, IEEE Photon. J. **7**, 6800407 (2015).
24. Y. Koike and M. Asai, NPG Asia Mater. **1**, 22 (2009).
25. Y. Mizuno and K. Nakamura, Appl. Phys. Lett. **97**, 021103 (2010).
26. Y. Mizuno, M. Kishi, K. Hotate, T. Ishigure, and K. Nakamura, Opt. Lett. **36**, 2378 (2011).
27. K. Minakawa, N. Hayashi, Y. Shinohara, M. Tahara, H. Hosoda, Y. Mizuno, and K. Nakamura, Jpn. J. Appl. Phys. **53**, 042502 (2014).